Zonal Wave 3 Pattern in the Southern Hemisphere generated by tropical convection

Rishav Goyal (rishav.goyal@unsw.edu.au)
ARC Centre of Excellence for Climate Extremes https://orcid.org/0000-0002-0307-4692

Martin Jucker
University of New South Wales https://orcid.org/0000-0002-4227-315X

Alex Sen Gupta
The University of New South Wales https://orcid.org/0000-0001-5226-871X

Harry Hendon
Bureau of Meteorology

Matthew England
Climate Change Research Centre (CCRC) https://orcid.org/0000-0001-9696-2930

Article

Keywords: Extratropical Atmospheric Circulation, Meridional Heat Transport, Antarctic Sea Ice Extent, Zonal Asymmetric Deep Atmospheric Convection, Hadley Cell

Posted Date: March 17th, 2021

DOI: https://doi.org/10.21203/rs.3.rs-320008/v1

Version of Record: A version of this preprint was published at Nature Geoscience on August 26th, 2021. See the published version at https://doi.org/10.1038/s41561-021-00811-3.

Zonal Wave 3 Pattern in the Southern Hemisphere generated by tropical convection

Rishav Goyal[1,2,*], Martin Jucker[1,2], Alex Sen Gupta[1,2], Harry H. Hendon[3] and Matthew H. England[1,2]

1. Climate Change Research Centre, University of New South Wales, NSW, 2052 Australia
2. ARC Centre of Excellence for Climate Extremes, University of New South Wales, NSW, Australia
3. Bureau of Meteorology, Melbourne, Australia

---

[*] *Corresponding author: rishav.goyal@unsw.edu.au*

Abstract

A distinctive feature of the Southern Hemisphere (SH) extratropical atmospheric circulation is the quasi-stationary zonal wave 3 (ZW3) pattern, characterized by three high and three low-pressure centers around the SH extratropics. This feature is present in both the mean atmospheric circulation and its variability on daily, seasonal and interannual timescales. While the ZW3 pattern has significant impacts on meridional heat transport and Antarctic sea ice extent, the reason for its existence remains uncertain, although it has long been assumed to be linked to the existence of three major land masses in the SH extratropics. Here we use an atmospheric general circulation model to show that the stationery ZW3 pattern is instead driven by zonal asymmetric deep atmospheric convection in the tropics, with little to no role played by the orography or land masses in the extratropics. Localized regions of deep convection in the tropics form a local Hadley cell which in turn creates a wave source in the subtropics that excites a poleward and eastward propagating wave train which forms stationary waves in the SH high latitudes. Our findings suggest that changes in tropical deep convection, either due to natural variability or climate change, will impact the zonal wave 3 pattern, with implications for Southern Hemisphere climate, ocean circulation, and sea-ice.

Introduction

The quasi-stationary ZW3 pattern is a prominent feature in the SH extratropical circulation, with significant impacts on Antarctic sea-ice[1,2], meridional heat and momentum transport[3] and CO_2 uptake[4]. The ZW3 pattern is evident in the time mean but exhibits seasonal variations in location and significant variability in both amplitude and phase at sub-monthly to monthly timescales[5,6]. ZW3 exhibits a quasi-stationary pattern with small longitudinal movement (between 15-25 degrees) between austral autumn and austral winter[3]. Previous

studies have suggested that the quasi-stationary ZW3 pattern evident in the time-mean circulation in the SH extratropics is linked to the land-ocean distribution in the SH mid-latitudes, in particular, the presence of three separated land masses and three ocean basins[2,3,7–10]. This conjecture seems plausible given the presence of the annual mean ZW3 surface pressure ridges on or near the southern flank of the three continents and troughs in the three ocean basins between them[3,7]. However, a similar stationary ZW3 pattern is also present in the Northern Hemisphere (NH) extratropics[11], where there is no obvious threefold symmetry in the land-ocean distribution. Therefore, the mechanisms responsible for the generation of this stationary ZW3 pattern in the SH extratropics require further examination.

Planetary wave activity in the SH extratropics is dominated by the presence of stationary ZW1 and ZW3 at sub-monthly to interannual timescales[5,6]. It has been suggested that ZW1 is maintained by both the Rossby wave activity that is forced from lower latitudes[12–16] and from the high orography of Antarctica[15,17,18]. ZW3 is a prominent feature in geopotential height and wind fields and dominates the zonally asymmetric extratropical circulation at sub-monthly[19,20], seasonal[21] and interannual timescales[22,23]. ZW3 also plays an important role in winter-time SH blocking events[24] and has been suggested to be the most persistent mode of SH eddy circulation[25]. The magnitude of the ZW3 pattern shows a maximum near 55°S and explains ~8% of variance in Empirical Orthogonal Function (EOF) analysis of monthly geopotential height south of 20°S[3] and greater than 45% of the variance in monthly meridional wind fields at 55°S[23].

ZW3 also plays an important role in the variability of meridional heat and momentum transport[3], and therefore has a substantial impact on Antarctic sea ice and SH extratropical climate[1,2]. The ZW3 pattern is evident in regression patterns of winds, sea level pressure,

and geopotential height onto the Southern Annular Mode (SAM) index; with the SAM representing the major mode of climate variability in the SH on monthly and interannual timescales (Fig.1a). The ZW3 pattern is also a prominent feature in the projected future mean sea level pressure changes in the SH extratropics (Fig. 1b). In recent years, extremes in the strength of the ZW3 pattern have been linked to the unprecedented 2015-16 Antarctic sea-ice decline[26–28] and the SH blocking highs[29]. Given the importance of the ZW3 pattern for Antarctic and SH climate, it is important to understand the generation and maintenance of this persistent atmospheric pattern in the SH extratropics. While the presence of this pattern in the SH has been previously linked to the land-ocean distribution in the extratropics[2,3,7–10], there has been no previous modelling work that substantiates this explanation. In this study, we undertake a series of sensitivity experiments using an Atmospheric General Circulation Model (AGCM) subject to different land-ocean configurations to uncover the mechanisms responsible for generating a stationary ZW3 pattern in the SH extratropics.

Experimental setup

We use the National Center for Atmospheric Research (NCAR) Community Earth System Model (CESM v1.2.2) which was part of the Coupled Model Intercomparison Project 5 (CMIP5). All model simulations are forced by prescribed sea surface temperatures (SST) and sea-ice and include active atmospheric and land model components. The control model experiment includes globally realistic land masses and orography, and climatologically and geographically varying SST forcing. A series of simulations is then configured with different land-ocean and SST configurations to examine the mechanisms that generate the stationary ZW3 in the SH extratropics (Methods), building up in complexity from a simple aquaplanet simulation with zonally uniform SST forcing. The subsequent experiments then include

additional tropical, extratropical, and polar land masses and orography relative to the control experiment.

Based on a first order comparison, the control simulation captures the pattern and magnitude of the ZW3 reasonably well compared to the European Centre for Medium Range Weather Forecasts (ECMWF) Reanalysis (ERA-Interim[30], Fig. S1a, S1b). While the magnitude of the modeled ZW3 is weaker than that estimated from the ERA-Interim reanalysis, this is a common problem with CMIP-type simulations, which systematically underestimate the amplitude of ZW3 in the SH[1]. Comparison across different Atmospheric Model Intercomparison Project (AMIP) simulations of CMIP5 models, that use the observed sea surface temperature and sea-ice boundary conditions, shows that the CESM model simulates both the amplitude and phase of the ZW3 pattern in the SH extratropics reasonably well (see Fig. S1c for a model intercomparison).

Results

Fourier analysis is used to separate the wave activity associated with each zonal wavenumber across the experimental set. Stationary waves are defined as the time-mean component of each wave. Therefore, by definition, a purely random wave (having different phases at different timesteps) will have zero stationary wave component. In order to build our understanding of the factors important for ZW3, we first analyze the aquaplanet simulation (Methods). Using monthly averaged data, only waves with zonal wavenumbers $k \leq 5$ are present (higher wavenumbers become important at shorter timescales than are retained by monthly averaging). Wave 5 dominates the 300 hPa meridional wind fields north of ~50°S, with maximum strength between 30-40°S (supplementary Fig. S2a). This agrees well with previous studies,[31–34] and these waves are believed to be trapped within the jet

stream and to be maintained by baroclinic energy conversion[34]. However, waves in the aquaplanet simulation are not phase locked i.e., they possess random phases at different times (Fig. 2a, supplementary Fig. S3; see caveat below). Indeed, the lack of zonal asymmetry in the aquaplanet should preclude any phase locking of the waves; however, a weak phase locking can be seen. This likely relates to the finite radiation timestep used in the model, which creates asymmetries because of the sun warming the same locations after a certain fixed interval of time, leading to small zonal asymmetries in solar heating. The resulting time mean ZW3 signal is however more than an order of magnitude smaller than the signals found in subsequent experiments.

To understand the role of SH landmasses in creating and maintaining a phase locked ZW3 pattern, we next add a single flat (at sea level) landmass to the aquaplanet configuration (Fig. 2b; see methods for details). We choose South America as it extends the furthest towards the south, has a tropical extension and also has the highest topography (i.e., the Andes) among the three landmasses in the SH midlatitudes. The wave energy in this simulation shifts to lower wavenumbers compared to the aquaplanet simulation (supplementary Fig. S2a) with ZW1 and ZW3 now dominating, and very little energy at wavenumbers 4 and above (supplementary Fig. S2b). A clear stationary (phase locked) ZW3 is now apparent with an amplitude comparable to the control simulation, although the phase is different (Fig. 2b). This suggests that a single land mass in the SH can generate a phase locked ZW3 pattern. Longer waves (i.e., ZW1 and ZW2) are also phase locked in this simulation (supplementary Fig. S4).

To examine whether the meridional location of the land mass is important to generate a stationary ZW3 structure, two additional simulations are next investigated, one with only the

tropical part of the South American land mass and another with only the extratropical South American land (Fig. 2c, 2d and methods). These simulations reveal that a stationary ZW3 pattern is only present in the tropical land mass simulation (with amplitude and phase almost identical to the simulation with all of South America present; Fig. 2c); conversely, in the midlatitude-only simulation, the wave phase is almost random (only a weak stationary ZW3 is present with similar phase and amplitude to the aquaplanet experiment; Fig. 2a and 2d). These simulations suggest that while a land mass in the extratropics plays little role in generating a stationary ZW3 pattern, a single land mass in the tropics is sufficient to generate a large amplitude stationary ZW3.

In the above experiments the land masses were all added without orography (i.e., flat land masses at sea level). To examine if the presence of three land masses in the SH extratropics can generate a phase locked ZW3 in a more realistic configuration, we next examine a simulation in which three extratropical land masses are all present with realistic orography (i.e., SA, Africa and Australia, added south of 20°S; Fig. 2e). Mountains are known to play an important role in creating phase locked zonal waves in the NH extratropics, particularly due to the presence of the Rockies and the Plateau of Tibet[35]. Even though there are fewer high orographic features in the SH, the Andes are as high as 2900 meters south of 20°S in the model and may play a role in phase locking the waves, such as the wavenumber 3 pattern. Yet in this simulation with added extratropical land masses and orography, there is no enhanced stationary ZW3 over and above that seen in the aquaplanet (Fig. 2e). The ZW3 signal present in this simulation possesses a random phase in time i.e., it is not stationary. The model resolution precludes orography of the Andes that precisely matches the real world (2900-m in the model compared to 3400-m in reality), however, recent studies[36] have found that the Andes being lower in coarse-resolution models has little effect on the wave

activity in the SH. This indicates that the presence of SH extratropical land masses (including orography) does not play a primary role in generating the phase locked ZW3 pattern in the SH extratropics; the Andes have too narrow a longitude range to generate a strong stationary wave as compared to their NH counterparts, where the mountains are higher and have much larger zonal extent. This finding is in contrast to the hypothesis put forward in previous studies[2,3,7–10].

ZW3 is also phase locked in other experiments we tested with tropical land masses added elsewhere (e.g., Africa, the maritime continent), with the resulting phases and amplitudes differing across these simulations compared to the tropical South America simulation (supplementary Fig. S5). We hypothesize that the tropical-extratropical teleconnection relates to deep adiabatic heating in the tropics that can be generated by any of the landmasses but also by warm tropical SSTs. This will be examined in the next section.

Finally, Antarctica is known to generate the stationary ZW1 in the SH extratropics[15,17,18], however, it is not thought to generate a stationary phase locked ZW3 pattern in the SH extratropics[37]. This has been confirmed in an additional experiment where we added Antarctica with orography to the aquaplanet configuration (supplementary Fig. S6). This experiment shows a stationary ZW1, but no stationary ZW3 is found in this simulation (supplementary Fig. S6).

Mechanism to generate stationary ZW3

We now elucidate how a localised zonal asymmetry in the tropics can generate a stationary ZW3 pattern in the extratropics. We begin by examining the tropical SA experiment in more detail. The presence of land in the tropics therefore provides a low-level perturbation to the

otherwise zonally uniform flow and results in convergence at the surface over the land mass. This low-level convergence causes convective heating in the atmosphere (supplementary Fig. S7) which results in enhanced upward motion (Fig. 3a) and divergence with an associated anticyclonic vorticity anomaly at upper levels (Fig. 3b). The response in the lower troposphere is similar to a Gill-type response[38] for a heat source in the tropics with two cyclonic circulations present on either side of the Equator (Fig. 3c). The lower-level perturbation is mostly confined near the heating source and has a weaker response in the extratropics; however, this is not the case in the upper troposphere where strong perturbations extend farther into the SH extratropics (Fig. 3b and 3c). The source (land mass) is present in the tropics where the mean flow is easterly, however, Rossby waves need westerly flow to propagate. This gap is bridged by the divergence in the upper tropospheric flow in the tropics, which results in sinking motion in the subtropics forming a local Hadley cell (Fig. 3a). This results in upper level convergence in the subtropics which then acts as a Rossby wave source because of the presence of westerlies in the subtropics[13]. In the upper troposphere (at 300 hPa), a wave train is set up poleward and eastward of the source region (Fig. 3b). This is similar to the wave train dynamics described by Hoskins and Karoly (1981)[12] for a subtropical heating source and by Trenberth et al (1998)[13] for a tropical heating source. These eastward and poleward propagating waves (supplementary Fig. S8) reflect from the high latitudes where the meridional gradient of absolute vorticity approaches zero, and then decay in the tropics where the zonal wind is zero[12]. The lowest wavenumbers ($k \leq 3$) have the strongest meridional group velocities so can propagate further poleward[12,13] before being reflected back to the tropics (Fig. 3b). The response is basically a dispersive Rossby wave train with each wavenumber following a different ray path[12]. The lowest wavenumber (ZW1) therefore travels the furthest poleward followed by progressively higher wavenumbers, which then create stationary zonal waves in

the SH extratropics (supplementary Fig. S9). The stationary wavenumber (Ks) profile in the SH (supplementary Fig. S9) suggests that wavenumber 3 is the dominant wavenumber in the SH extratropical region (between 50°S-65°S), which explains why ZW3 dominates in this latitude band.

The eastward and poleward propagating wave train from the poleward flank of the heating source generates stationary waves in the SH with a stationary (phase locked) ZW3 present in the extratropics, with a maximum near 55°S (Fig. 3d and 3e). This wave train structure has been observed in previous studies using simple barotropic and baroclinic models with prescribed diabatic heating anomalies[12,13]. However, here we use a more sophisticated atmospheric general circulation model which is known to simulate realistic atmospheric stationary waves[9,39]. These poleward moving wave trains are absent in all simulations we consider unless a source of zonal asymmetry in the deep convection is present in the tropics. Without any tropical zonal asymmetry, there are no upper-level changes generated to drive a poleward propagating Rossby wave (supplementary Fig. S10). This is likely due to the lack of deep convection in mid-latitudes[12] (Fig. S10a). While a low-level perturbation (heating) is balanced by strong vertical advection in the tropics, in the mid-latitudes, it is balanced by horizontal advection of cold air from polar latitudes near the surface[40].

Changing the location and extent of the land mass in the tropics experiments in turn changes the location and extent of maximum deep convection - and hence the location of the Rossby wave source in the subtropics - which in turn changes the phase of the ZW3 pattern in the SH extratropics (supplementary Fig. S5). In other words, the phase of the ZW3 pattern is dependent on the longitudinal location of the Rossby wave source in the tropics. The combined effect is however non-linear, i.e., the amplitude of the combined ZW3 for all

three individual tropical land mass cases is different to that of the full tropical land mass simulation (supplementary Fig. S5).

While the above experiments use an idealized landmass to provide a tropical source of heating, the strongest tropical heating actually occurs over the Indo-Pacific warm pool and therefore acts as the strongest source of deep convection in the tropics (refer to vertical velocity in *CTRL*, Fig. S11a). An additional experiment ($Tropics_{land+SST}$) is carried out which has a realistic tropical configuration with landmasses and climatological SSTs between 10°S - 10°N and zonally uniform setup everywhere else (refer to Fig. 2f and methods for details). A clear stationary ZW3 pattern is found in this simulation (Fig. 2f), with higher amplitude than the previous simulations that included just tropical landmasses, and similar in magnitude to the CTRL run. This suggests that convection over the Indo-Pacific warm pool has a strong role in generating the stationary ZW3 in the SH extratropics. We note that a wave train also propagates into the Northern Hemisphere and may play a role in ZW3 formation (Fig. 2f), although the higher and more extensive Tibetan plateau and Rockies may also be important[35]. Small differences in the ZW3 in $Tropics_{land+SST}$ simulation as compared to CTRL simulation are expected because the mean circulation in this simulation is slightly different to CTRL because of the absence of realistic extratropical landmasses, and because the refractive effects on the waves are determined by the mean atmospheric circulation (Fig. S9).

In summary, the presence of zonal asymmetries in deep convection in the tropics acts as a stationary source of wave activity. The wave travels eastward and poleward from the source region (Indo-Pacific warm pool) generating phase locked zonal waves in the SH extratropics.

In addition to ZW3, the other low frequency waves which dominate the wave spectrum (i.e., ZW1 and 2) are also phase locked in simulations with a tropical source of deep convection.

Summary and conclusions

Using atmospheric general circulation model simulations, we have examined the factors responsible for generating the stationary ZW3 pattern in the SH extratropics. We show that contrary to widely held opinion, the presence of three land masses in the SH extratropics is not the primary cause of the stationary (phase locked) ZW3 pattern. Instead, the presence of a single localized source of deep convection in the tropics (in particular over the Indo-Pacific warm pool) is sufficient to generate Rossby waves in the SH extratropics that can set up a stationary ZW3 structure. The teleconnection from the tropics to the extratropical latitudes is controlled by the upper level atmospheric flow, where the perturbation is provided by the presence of the lower boundary acting as a localized source of deep convection (Fig. 4). Deep convection in the tropics forms a local Hadley cell which subsides in the subtropics where westerlies are present. The localized upper level convergence generated because of the local Hadley cell generates a Rossby wave source in the subtropics. Rossby waves with strong meridional group velocities then move poleward from the subtropics and create phase-locked stationary zonal waves in the SH extratropics. The complete process that emerges is represented in a schematic shown in Fig. 4 and the supplementary animation. In contrast to this tropical driving mechanism, we found that neither the presence of extratropical land nor orography could generate significant phase locking of the stationary ZW3 pattern in the SH extratropics.

Our work suggests that the Indo-Pacific warm pool SSTs play a major role in generating a stationary ZW3. Indeed, a clear wave train is found to be propagating poleward and

eastward from the Indo-Pacific warm pool in the CTRL simulation (Fig. S11b). In addition to this, there is more than one source of convection in the tropics (Fig. S11) and these sources vary in time either because of changes in natural variability both at the shorter time scales such as the Madden Julian Oscillation (MJO) and monsoon variability, and at longer timescales such as El-Niño Southern Oscillation (ENSO) or the Indian Ocean Dipole (IOD), or because of climate change[39,41].

Zonal wave 3 also shows a strong variability at sub-monthly as well as seasonal timescales, with stronger ZW3 found during austral fall and winter and weaker ZW3 in spring and early summer[6]. Our work suggests that the climatological mean ZW3 pattern is strongly dependent not only on tropical deep convection but also on the background atmospheric circulation; it might further be expected that variability in ZW3 also depends on these two factors. This is analysed using a comparison of different AMIP model simulations (Fig. S1c, S1d), which show a similar spread in the bias in both the magnitude and phase as was found in the coupled CMIP5 model simulations. As the AMIP simulations are forced by the same observed SST and sea-ice fields, the presence of a similar bias across AMIP and CMIP simulations suggests that there are other factors at play apart from model SST differences. This is because wave propagation from the tropics to the extratropics is affected by the convective patterns simulated by each model, as well as the refractive effects of the background circulation (Fig. S9).

Our analysis suggests that any future changes in the ZW3 will be primarily dependent on changes in (a) tropical SST warming and (b) changes in the atmospheric circulation in the SH. Future warming of tropical SST is expected to weaken the tropical-extratropical teleconnections because of the projected weakening in tropical convective circulation in the

future[39]. Future warming of tropical SST is projected to result in upper tropospheric warming in the tropics, which in turn leads to an increase in the static stability in the tropics[39,41]. Increased static stability results in weaker vertical motions from increased SST warming and weaker upper-level divergence, which could lead to weaker tropical-extratropical teleconnections. Zonal winds in the SH extratropics are also projected to intensify with global warming[42]. Stationary wave theory implies that wavenumber scales inversely with the strength of the zonal flow, which therefore suggests a decrease in wavenumber in the future. While this is a simple assessment of expected future changes in the ZW3 pattern under global warming, uncertainties remain. For example, changes in the tropical wave source resulting from possible reorganization of convection in the tropics[43] and a projected poleward shift in the zonal winds in the SH extratropics[42] may also play a role in driving future changes in the ZW3 pattern. This has important implications for climate variability and climate change in the region.

Author contributions

R.G. conceived the study and along with M.J., A.S.G. and M.H.E. formulated the experimental design. R.G. conducted the atmospheric model simulations and produced all the analyses examined in the study. All authors contributed to interpreting the results, discussion of the associated dynamics and writing the paper.

Competing interests

The authors declare no competing financial interests

Methods

Climate Model

NCAR CESM v1.2.2 model is used with prescribed Sea Surface Temperatures (SSTs) and sea-ice. The atmospheric component of the model is the Community Atmosphere Model (CAM)[44] Version 4 and is coupled to the Community Land Model (CLM)[45] Version 4. CAM4 is run with a 1.875 x 2.5° finite volume grid with 26 hybrid sigma levels. The atmospheric composition and prescribed SSTs and sea-ice are set to a pre-industrial configuration.

Model experiments

Model simulations with CESM are carried out to understand the origin and maintenance of the stationary ZW3 in the SH extratropics. For all the simulations, the model uses pre-industrial levels of greenhouse gases, aerosols and other forcing. A control simulation (*CTRL*) is carried out with a repeat cycle of climatological monthly SSTs, sea-ice and ozone. The control simulation has a global realistic land-sea configuration as well as orography. An aquaplanet (*Aqua*) simulation is integrated in which land is removed everywhere (Fig. 2a) and ozone, SSTs and sea-ice are all set to zonally averaged monthly climatological fields. Another simulation is then carried out in which only South America (with orography removed) is added to the aquaplanet (Fig. 2b). In this experiment the presence of land alters the albedo and changes the surface fluxes because of the differences in the heat capacity, surface roughness and moisture availability over land as compared to the ocean. Separate experiments are then configured with land present only over tropical South America (between 10°S - 10°N, Fig. 2c) and only over South America poleward of 20° S (Fig. 2d), respectively. Another simulation is carried out in which land and orography over the three continents is present south of 20°S (Fig. 2e). The model resolution precludes having orography that precisely matches the real world. Nevertheless, the maximum height of the

mountains south of 20°S is similar to reality (2900 m in CESM and 3400 m in reality). Lastly, another simulation (*Tropics*$_{land+SST}$) is then integrated in which landmasses and climatological SSTs in the tropics between 10°S - 10°N are added to the zonally symmetric setup of the aquaplanet simulation (Fig. 2f). In all the simulations except *CTRL* and *Tropics*$_{land+SST}$, zonally symmetric monthly climatological SSTs and sea-ice are prescribed. In the control simulation, zonally varying monthly climatological SSTs and sea-ice are prescribed. All model simulations are integrated for 120 years. The first 20 years are discarded as a spin-up period and the remaining 100 years are used for the analyses presented here.

Analysis methods

Monthly mean geopotential height, zonal winds and meridional winds at different vertical levels are used to examine the horizontal and vertical structure of the eddy field in the SH. To isolate ZW3 variability we consider a band of geopotential height at 55°S and 300 hPa. Fourier analysis is used to separate the activity associated with each zonal wavenumber.

Other analysed data

Monthly averaged mean sea level pressure (MSLP) and geopotential height data from the European Centre for Medium Range Weather Forecasts (ECMWF) Reanalysis (ERA-Interim)[30], ECMWF Reanalysis (ERA-5)[46] National Centre for Environmental Prediction-National Centre for Atmospheric Research (NCEP-NCAR) reanalysis[47] from 1979-2008 are used in the study. MSLP and 850 hPa winds from the coupled model runs of the Community Earth System Model (CESM) which were submitted to Coupled Model Intercomparison Project 5 (CMIP5) are also analysed. CESM model data from 8 ensembles of the historical (1900-2005) as well as 8 ensembles of the RCP8.5 (2006-2100) simulations are analysed in this study. 300 hPa geopotential height fields from the pre-industrial control simulations of 18

CMIP5 models and Atmospheric Model Intercomparison Project (AMIP) simulations from 23 CMIP5 models are also used in this study.

Data Availability Statement

ERA-Interim data used in the study can be downloaded from https://apps.ecmwf.int/datasets/data/interim-full-moda/levtype=sfc/. The data generated from the model simulations will receive a DOI and will be made available using a public repository.

Code Availability Statement

Python scripts used for the analysis described in this study can be obtained from the corresponding author upon reasonable request.

References

1. Raphael, M. N. The influence of atmospheric zonal wave three on Antarctic sea ice variability. *J. Geophys. Res.* **112**, D12112 (2007).
2. Raphael, M. N. & Hobbs, W. The influence of the large-scale atmospheric circulation on Antarctic sea ice during ice advance and retreat seasons. *Geophys. Res. Lett.* **41**, 5037–5045 (2014).
3. Raphael, M. N. A zonal wave 3 index for the Southern Hemisphere. *Geophys. Res. Lett.* **31**, (2004).
4. Keppler, L. & Landschützer, P. Regional Wind Variability Modulates the Southern Ocean Carbon Sink. *Sci. Rep.* **9**, 7384 (2019).
5. Renwick, J. A. Persistent Positive Anomalies in the Southern Hemisphere Circulation. *Mon. Weather Rev.* **133**, 977–988 (2005).
6. Turner, J., Hosking, J. S., Bracegirdle, T. J., Phillips, T. & Marshall, G. J. Variability and trends in the Southern Hemisphere high latitude, quasi-stationary planetary waves. *Int. J. Climatol.* **37**, 2325–2336 (2017).
7. van Loon, H. & Jenne, R. L. The zonal harmonic standing waves in the southern hemisphere. *J. Geophys. Res.* **77**, 992–1003 (1972).
8. Lejenas, H. Southern Hemisphere Planetary-scale Waves and Blocking. *J. Meteorol. Soc. Japan. Ser. II* **66**, 777–781 (1988).
9. Raphael, M. N. Quasi-Stationary Waves in the Southern Hemisphere: An Examination of Their Simulation by the NCAR Climate System Model, with and without an Interactive Ocean*. *J. Clim.* **11**, 1405–1418 (1998).
10. Yuan, X. & Li, C. Climate modes in southern high latitudes and their impacts on Antarctic sea ice. *J. Geophys. Res.* **113**, C06S91 (2008).
11. Teng, H. & Branstator, G. A Zonal Wavenumber 3 Pattern of Northern Hemisphere Wintertime Planetary Wave Variability at High Latitudes. *J. Clim.* **25**, 6756–6769 (2012).
12. Hoskins, B. J. & Karoly, D. J. The Steady Linear Response of a Spherical Atmosphere to Thermal and Orographic Forcing. *J. Atmos. Sci.* **38**, 1179–1196 (1981).
13. Trenberth, K. E. *et al.* Progress during TOGA in understanding and modeling global teleconnections associated with tropical sea surface temperatures. *J. Geophys. Res. Ocean.* **103**, 14291–14324 (1998).
14. Inatsu, M. & Hoskins, B. J. The Zonal Asymmetry of the Southern Hemisphere Winter Storm Track. *J. Clim.* **17**, 4882–4892 (2004).
15. Quintanar, A. I. & Mechoso, C. R. Quasi-Stationary Waves in the Southern Hemisphere. Part II: Generation Mechanisms. *J. Clim.* **8**, 2673–2690 (1995).
16. Peña-Ortiz, C., Manzini, E. & Giorgetta, M. A. Tropical Deep Convection Impact on Southern Winter Stationary Waves and Its Modulation by the Quasi-Biennial Oscillation. *J. Clim.* **32**, 7453–7467 (2019).
17. James, I. N. On the forcing of planetary-scale Rossby waves by Antarctica. *Q. J. R. Meteorol. Soc.* **114**, 619–637 (1988).
18. Watterson, I. G. & James, I. N. Baroclinic Waves Propagating From A High-Latitude Source. *Q. J. R. Meteorol. Soc.* **118**, 23–50 (1992).
19. Mo, K. C. & Ghil, M. Statistics and Dynamics of Persistent Anomalies. *J. Atmos. Sci.* **44**, 877–902 (1987).
20. Hansen, A. R. & Sutera, A. Planetary-Scale Flow Regimes in Midlatitudes of the Southern Hemisphere. *J. Atmos. Sci.* **48**, 952–964 (1991).
21. Mo, K. C. & White, G. H. Teleconnections in the Southern Hemisphere. *Mon. Weather Rev.* **113**, 22–37 (1985).
22. Trenberth, K. E. Planetary Waves at 500 mb in the Southern Hemisphere. *Mon. Weather Rev.* **108**, 1378–1389 (1980).
23. Irving, D. & Simmonds, I. A Novel Approach to Diagnosing Southern Hemisphere Planetary Wave Activity and Its Influence on Regional Climate Variability. *J. Clim.* **28**,

9041–9057 (2015).

24. Trenberth, K. F. & Mo, K. C. Blocking in the Southern Hemisphere. *Mon. Weather Rev.* **113**, 3–21 (1985).
25. Mo, K. C. Quasi-Stationary States in the Southern Hemisphere. *Mon. Weather Rev.* **114**, 808–823 (1986).
26. Wang, G. *et al.* Compounding tropical and stratospheric forcing of the record low Antarctic sea-ice in 2016. *Nat. Commun.* **10**, 13 (2019).
27. Purich, A. & England, M. H. Tropical Teleconnections to Antarctic Sea Ice During Austral Spring 2016 in Coupled Pacemaker Experiments. *Geophys. Res. Lett.* **46**, 6848–6858 (2019).
28. Meehl, G. A. *et al.* Sustained ocean changes contributed to sudden Antarctic sea ice retreat in late 2016. *Nat. Commun.* **10**, 14 (2019).
29. Hobbs, W. R. & Raphael, M. N. Characterizing the zonally asymmetric component of the SH circulation. *Clim. Dyn.* **35**, 859–873 (2010).
30. Dee, D. P. *et al.* The ERA-Interim reanalysis: configuration and performance of the data assimilation system. *Q. J. R. Meteorol. Soc.* **137**, 553–597 (2011).
31. Hendon, H. H. & Hartmann, D. L. Variability in a Nonlinear Model of the Atmosphere with Zonally Symmetric Forcing. *J. Atmos. Sci.* **42**, 2783–2797 (1985).
32. Robinson, W. The dynamics of the zonal index in a simple model of the atmosphere. *Tellus A* **43**, 295–305 (1991).
33. Watanabe, M. On the presence of annular variability in an aquaplanet model. *Geophys. Res. Lett.* **32**, L05701 (2005).
34. Zappa, G., Lucarini, V. & Navarra, A. Baroclinic Stationary Waves in Aquaplanet Models. *J. Atmos. Sci.* **68**, 1023–1040 (2011).
35. Held, I. M., Ting, M. & Wang, H. Northern Winter Stationary Waves: Theory and Modeling. *J. Clim.* **15**, 2125–2144 (2002).
36. Garfinkel, C. I., White, I., Gerber, E. P. & Jucker, M. The Impact of SST Biases in the Tropical East Pacific and Agulhas Current Region on Atmospheric Stationary Waves in the Southern Hemisphere. *J. Clim.* **33**, 9351–9374 (2020).
37. Baines, P. G. & Fraedrich, K. Topographic Effects on the Mean Tropospheric Flow Patterns around Antarctica. *J. Atmos. Sci.* **46**, 3401–3415 (1989).
38. Gill, A. E. Some simple solutions for heat-induced tropical circulation. *Q. J. R. Meteorol. Soc.* **106**, 447–462 (1980).
39. Wills, R. C. J., White, R. H. & Levine, X. J. Northern Hemisphere Stationary Waves in a Changing Climate. *Curr. Clim. Chang. Reports* **5**, 372–389 (2019).
40. Held, I. M. The Vertical Scale of an Unstable Baroclinic Wave and Its Importance for Eddy Heat Flux Parameterizations. *J. Atmos. Sci.* **35**, 572–576 (1978).
41. Müller, W. A. & Roeckner, E. ENSO teleconnections in projections of future climate in ECHAM5/MPI-OM. *Clim. Dyn.* **31**, 533–549 (2008).
42. Goyal, R., Sen Gupta, A., Jucker, M. & England, M. H. Historical and Projected Changes in the Southern Hemisphere Surface Westerlies. *Geophys. Res. Lett.* **48**, e2020GL090849 (2021).
43. Kent, C., Chadwick, R. & Rowell, D. P. Understanding Uncertainties in Future Projections of Seasonal Tropical Precipitation. *J. Clim.* **28**, 4390–4413 (2015).
44. Neale, R. B. *et al.* Description of the NCAR Community Atmosphere Model (CAM 4.0). *NCAR Tech. Note* **TN-485**, 1–196 (2010).
45. Oleson W Keit, Lawrence M David, Bonan B Gordon, Flanner G Mark, Kluzek Erik, Lawrence J Peter, Levis Samuel, Swenson C Sean, T. E. P. Technical Description of version 4.0 of the Community Land Model (CLM). *NCAR Tech. Note* **TN-478**, 1–238 (2010).
46. Hersbach, H. *et al.* The ERA5 global reanalysis. *Q. J. R. Meteorol. Soc.* **146**, 1999–2049 (2020).
47. Kalnay, E. *et al.* The NCEP/NCAR 40-Year Reanalysis Project. *Bull. Am. Meteorol. Soc.* **77**, 437–472 (1996).

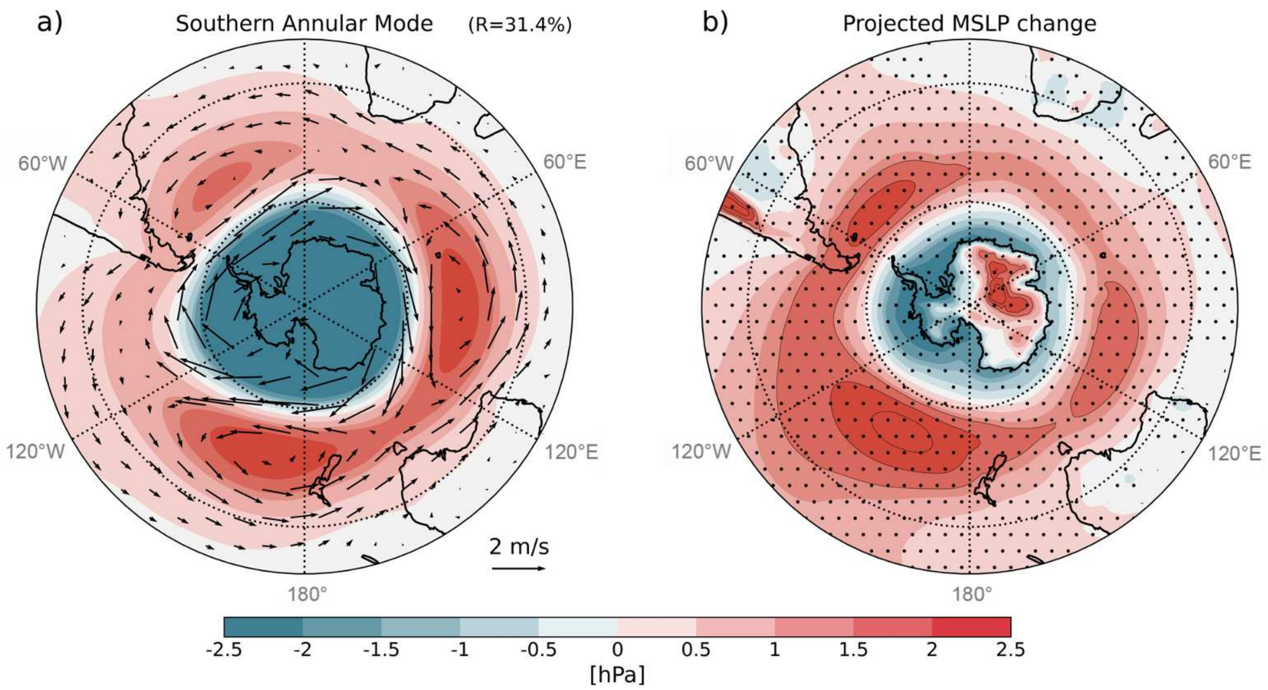

Figure 1 | Sea level pressure variability and projected 21st Century change in the Southern Hemisphere extratropics. Shading in panel a) shows Southern Annular Mode (SAM) obtained from the average of 8 ensembles of coupled CESM model runs for the historical time-period from 1900-2005. Vectors represent regression of the SAM index onto surface winds. The SAM is defined here as the leading empirical orthogonal function (EOF) of the mean sea level pressure (MSLP) south of 20°S and the SAM index is then taken as the principal component of the first EOF mode. Panel b) shows the difference between the climatological mean MSLP in the late 21st Century (2050-2100 average) and that in the late 20th Century (1950-2000 average). Stippling in (b) represent regions where differences are significant at the 95% confidence level.

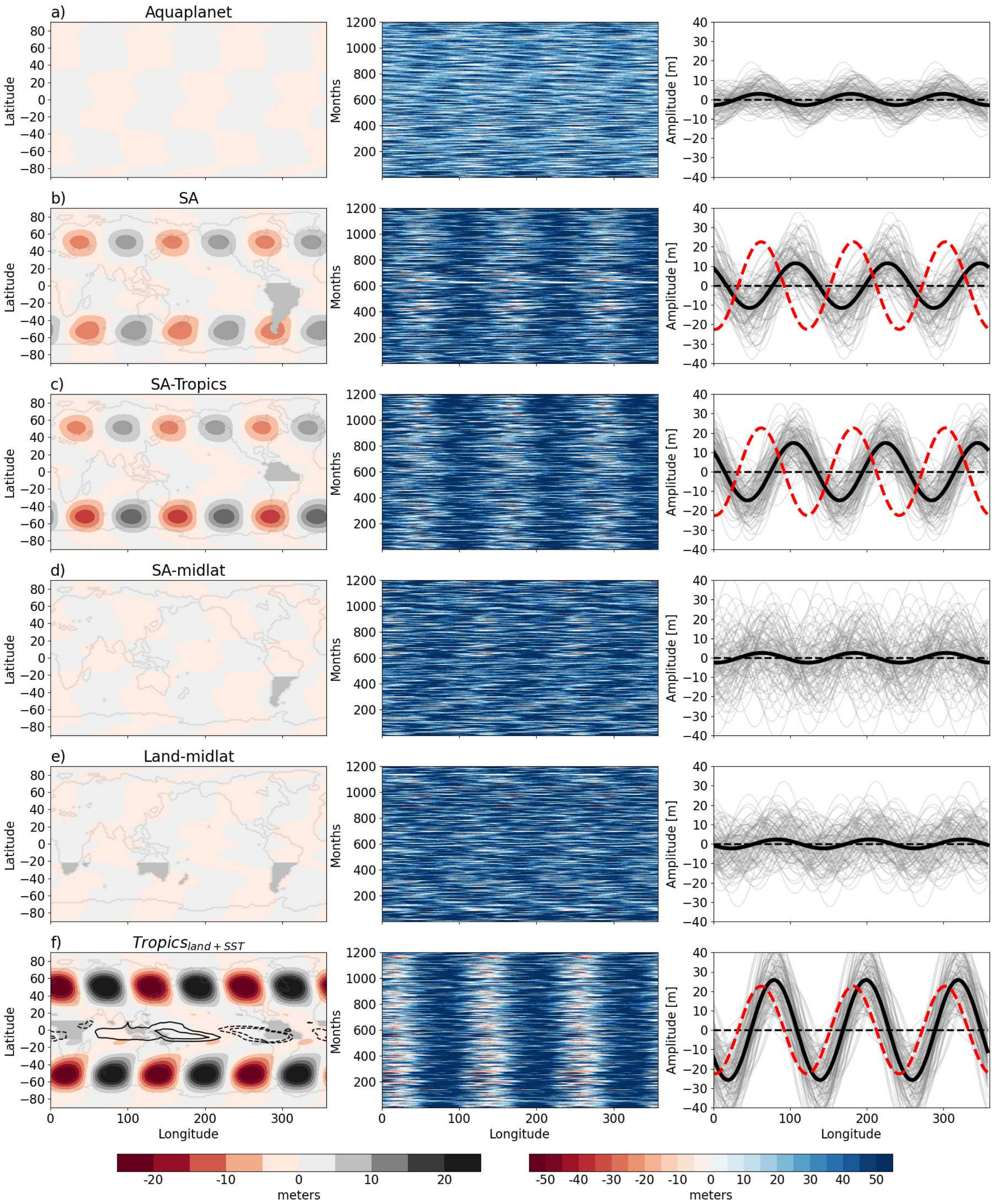

Figure 2 | Zonal wave 3 (ZW3) amplitude and phase in model simulations with different land-sea configuration. ZW3 phase and amplitude in a) aquaplanet, b) full South America, c) tropical South America, d) mid-latitude South America, e) land in SH midlatitudes (with orography) simulations and f) realistic tropics (land + SSTs) configuration. Grey shaded map regions in the left column shows the region where the land is present in each model simulation. Black contours in the first column of 2f) shows SST at 1°C intervals

after zonal mean has been removed. Shading in the first column shows the stationary (time mean) ZW3 component filtered from the 300 hPa geopotential height field. The middle column shows longitude-time Hovmöller plots for ZW3 at 55°S for each month for 100 years showing the time evolution of ZW3 phase and amplitude. The right column shows interannual variation in the ZW3 at 55°S with thin grey lines showing annual mean ZW3 for each year of the simulation (100 lines for 100 years), thick black line showing the mean over the entire 100-year period and dashed red line in 2f) shows mean over the entire 100-year period in control simulation. Dashed black line in the right column represents the zero line.

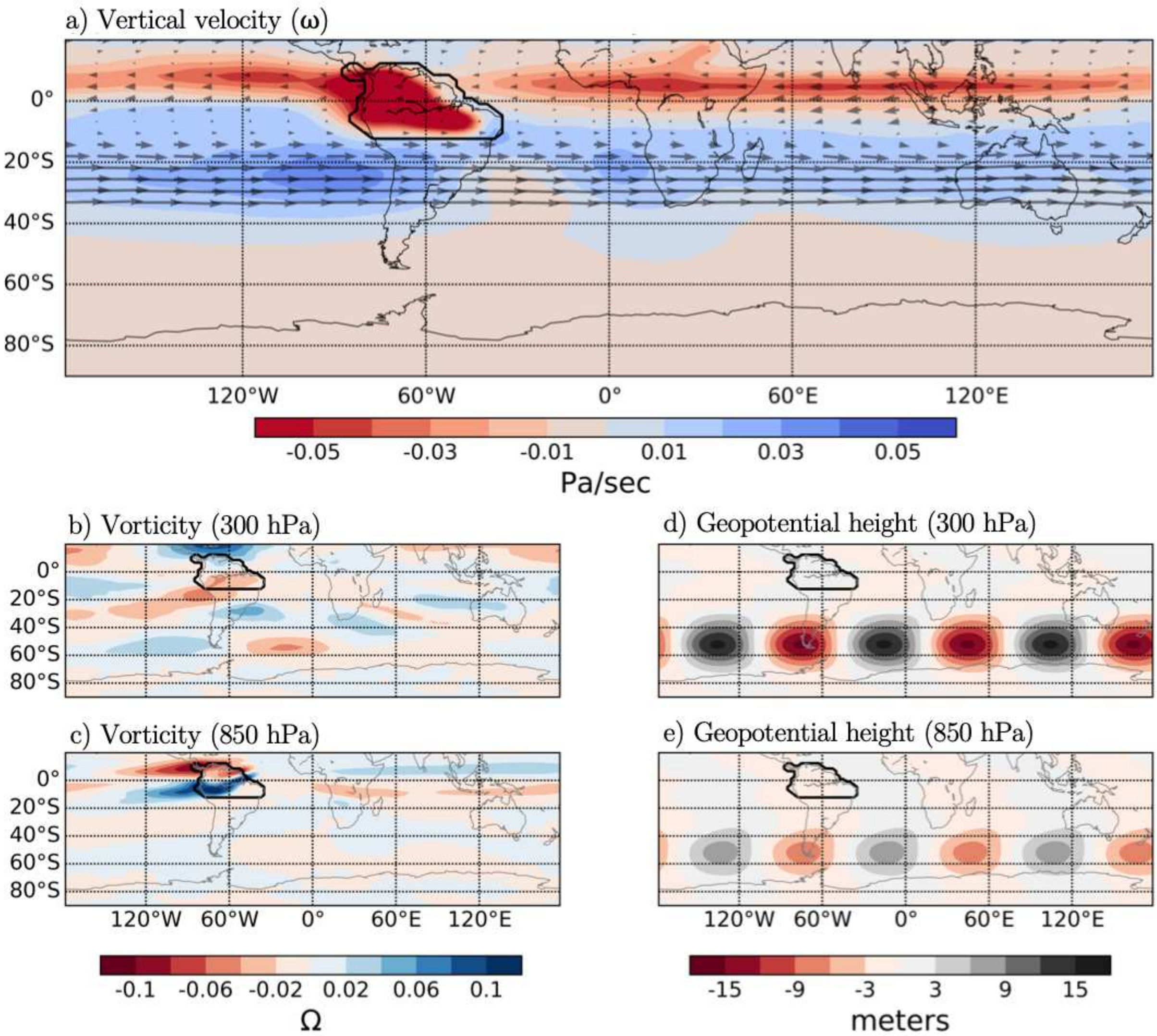

Figure 3 | Vertical velocity (omega), perturbation vorticity and geopotential height (corresponding to zonal wavenumber 3) for the tropical South America simulation. Shading in Panel a) shows vertical velocity (Pa/s) at 300 hPa and vectors show the zonal wind at 300 hPa between 35°S - 20°N. Panels b) and c) respectively show perturbation vorticity (units are Ω, where Ω =7.29x10^{-5} rad/sec, is the rotational rate of earth) at 300 hPa and 850 hPa. Panels d) and e) show the filtered zonal wavenumber 3 component in the geopotential height (in meters) at 300 hPa and 850 hPa respectively.

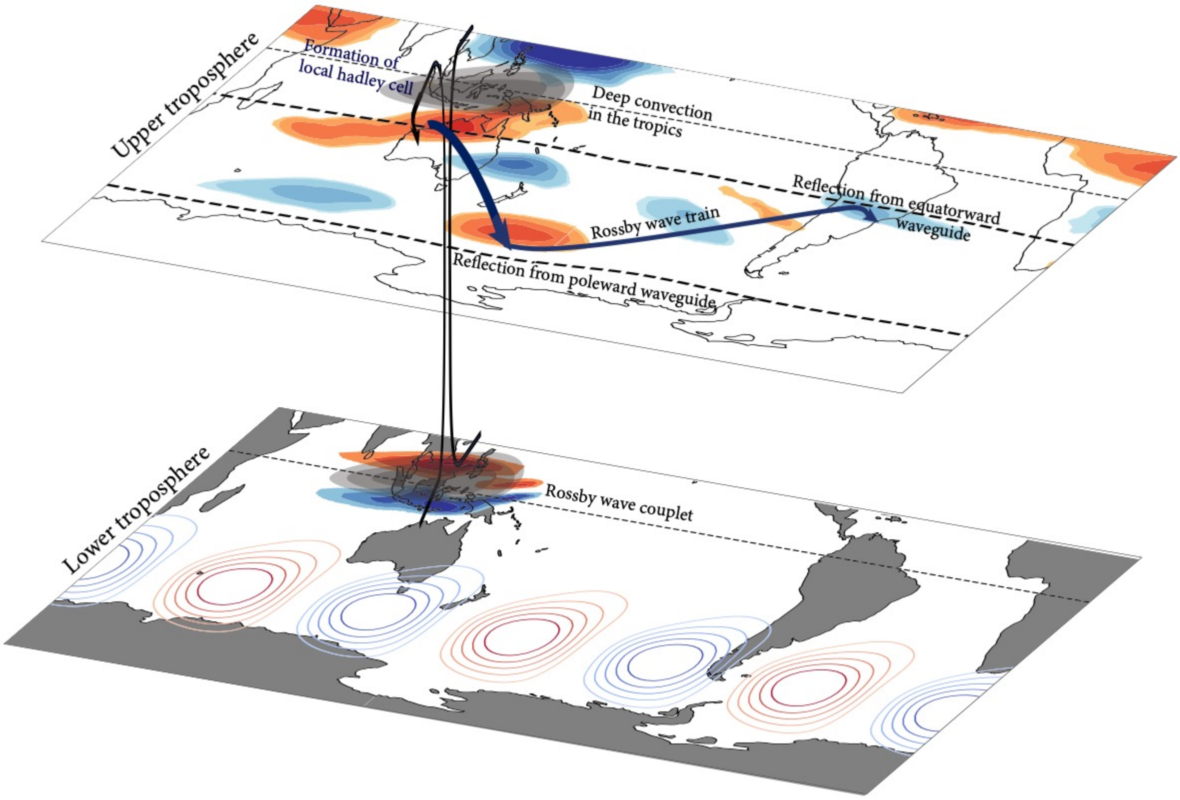

Figure 4 | Schematic summarizing the role of tropical convection in generating Zonal Wave 3 in the Southern Hemisphere extratropics. Grey shading represents outgoing longwave radiation (OLR) and the vertical arrows represent deep convection in the tropics. Perturbation vorticity is shown by the coloured shading representing a Rossby wave train travelling poleward and eastward from the source region before reflecting from the poleward and equatorward waveguides. The poleward and equatorward waveguides are represented by the thick dashed lines. Contours show the Fourier filtered zonal wave 3 from the 300hPa geopotential height field.

Figures

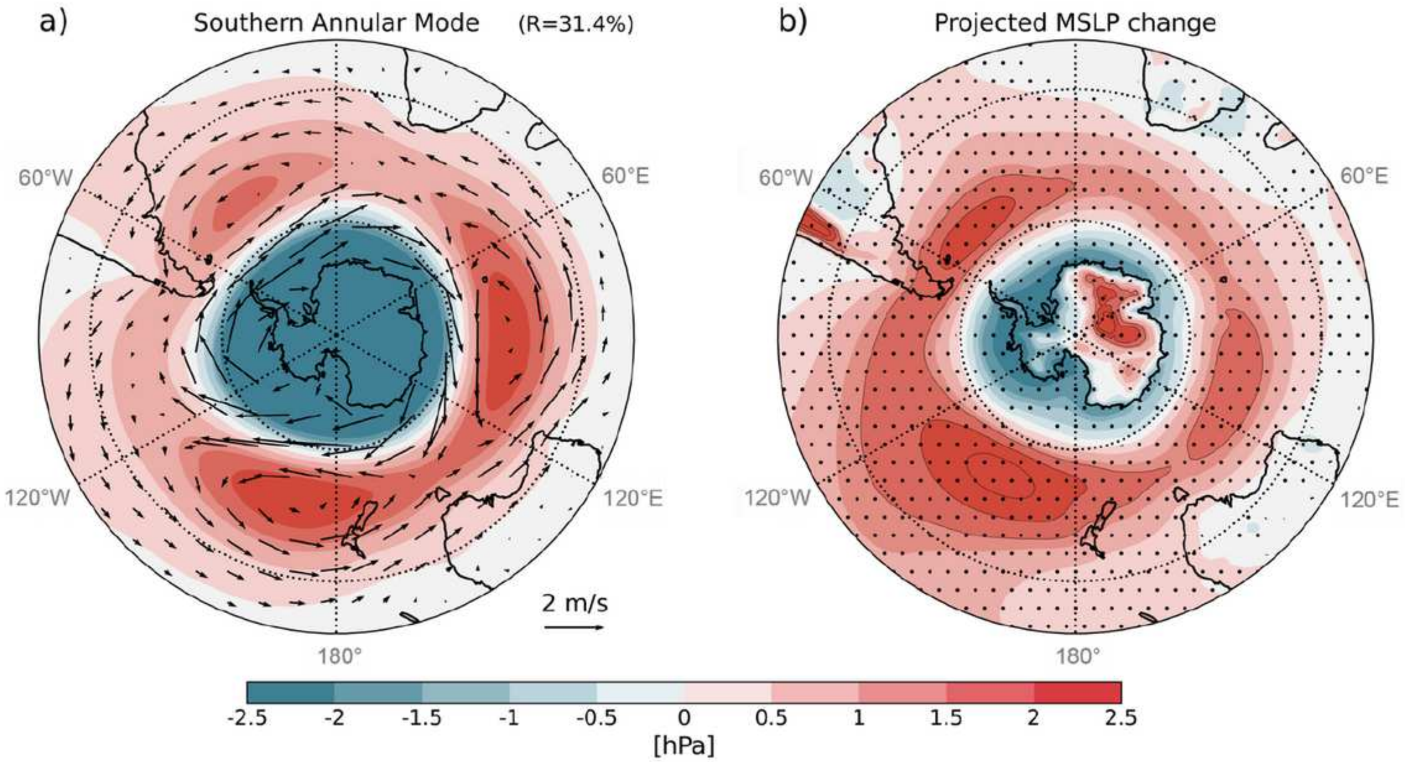

Figure 1

Sea level pressure variability and projected 21st Century change in the Southern Hemisphere extratropics. Shading in panel a) shows Southern Annular Mode (SAM) obtained from the average of 8 ensembles of coupled CESM model runs for the historical time-period from 1900-2005. Vectors represent regression of the SAM index onto surface winds. The SAM is defined here as the leading empirical orthogonal function (EOF) of the mean sea level pressure (MSLP) south of 20°S and the SAM index is then taken as the principal component of the first EOF mode. Panel b) shows the difference between the climatological mean MSLP in the late 21st Century (2050-2100 average) and that in the late 20th Century (1950-2000 average). Stippling in (b) represent regions where differences are significant at the 95% confidence level. Note: The designations employed and the presentation of the material on this map do not imply the expression of any opinion whatsoever on the part of Research Square concerning the legal status of any country, territory, city or area or of its authorities, or concerning the delimitation of its frontiers or boundaries. This map has been provided by the authors.

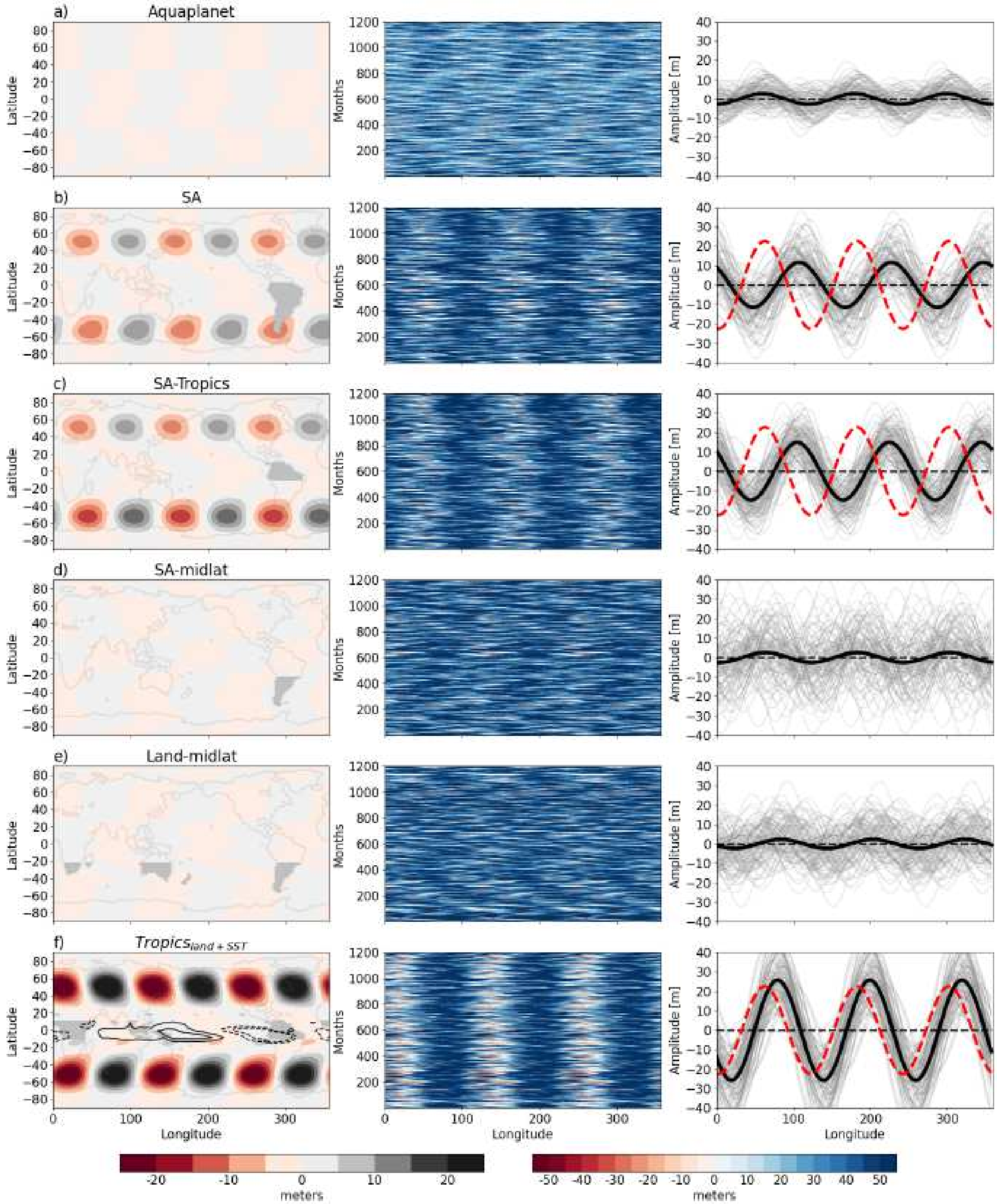

Figure 2

Zonal wave 3 (ZW3) amplitude and phase in model simulations with different land-sea configuration. ZW3 phase and amplitude in a) aquaplanet, b) full South America, c) tropical South America, d) mid-latitude South America, e) land in SH midlatitudes (with orography) simulations and f) realistic tropics (land + SSTs) configuration. Grey shaded map regions in the left column shows the region where the land is present in each model simulation. Black contours in the first column of 2f) shows SST at 1°C intervals

after zonal mean has been removed. Shading in the first column shows the stationary (time mean) ZW3 component filtered from the 300 hPa geopotential height field. The middle column shows longitude-time Hovmöller plots for ZW3 at 55°S for each month for 100 years showing the time evolution of ZW3 phase and amplitude. The right column shows interannual variation in the ZW3 at 55°S with thin grey lines showing annual mean ZW3 for each year of the simulation (100 lines for 100 years), thick black line showing the mean over the entire 100-year period and dashed red line in 2f) shows mean over the entire 100-year period in control simulation. Dashed black line in the right column represents the zero line. Note: The designations employed and the presentation of the material on this map do not imply the expression of any opinion whatsoever on the part of Research Square concerning the legal status of any country, territory, city or area or of its authorities, or concerning the delimitation of its frontiers or boundaries. This map has been provided by the authors.

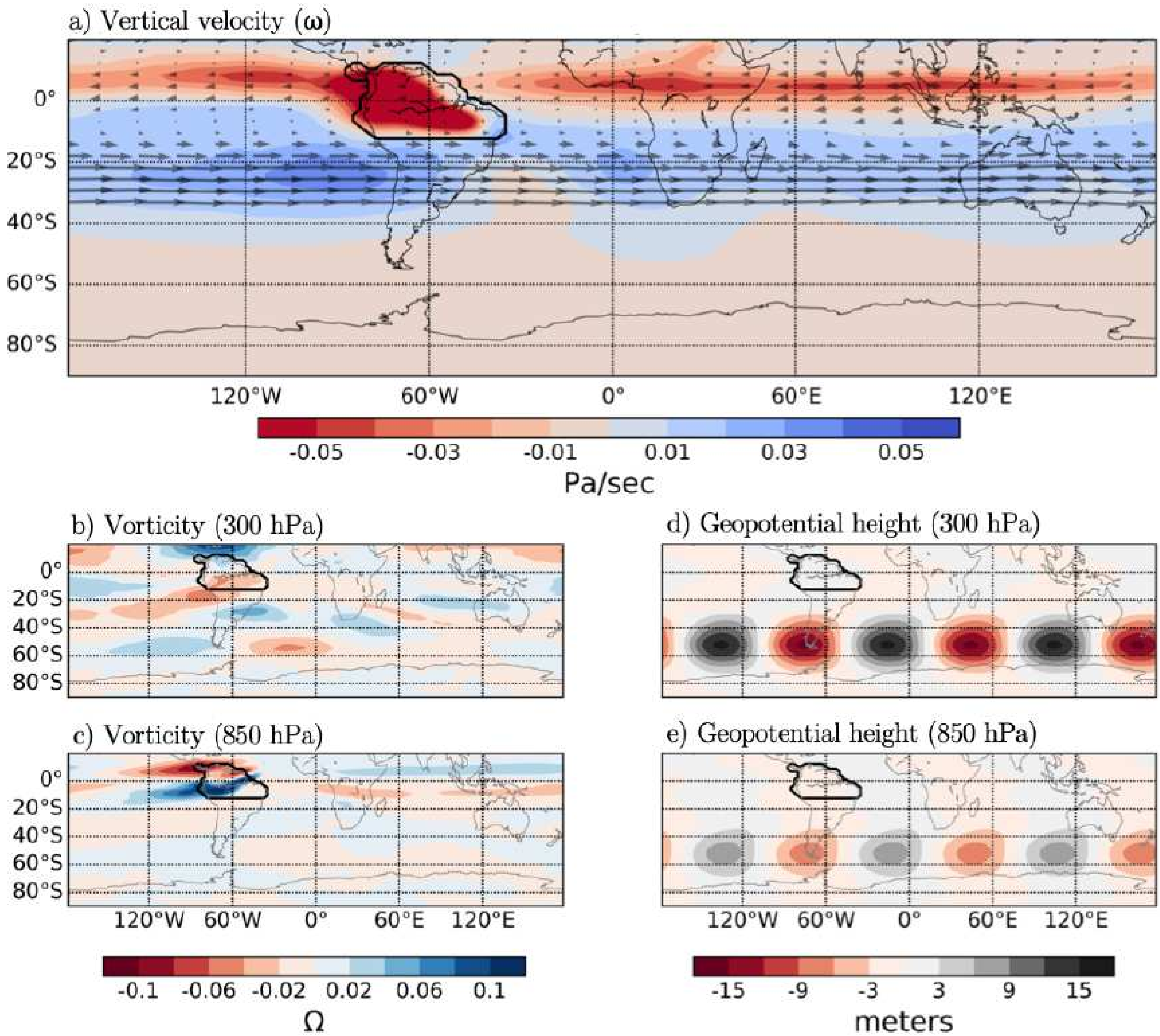

Figure 3

Vertical velocity (omega), perturbation vorticity and geopotential height (corresponding to zonal wavenumber 3) for the tropical South America simulation. Shading in Panel a) shows vertical velocity (Pa/s) at 300 hPa and vectors show the zonal wind at 300 hPa between 35°S - 20°N. Panels b) and c) respectively show perturbation vorticity (units are W, where W =7.29x10-5 rad/sec, is the rotational rate of earth) at 300 hPa and 850 hPa. Panels d) and e) show the filtered zonal wavenumber 3 component in the geopotential height (in meters) at 300 hPa and 850 hPa respectively. Note: The designations employed and the presentation of the material on this map do not imply the expression of any opinion whatsoever on the part of Research Square concerning the legal status of any country, territory, city or area or of its authorities, or concerning the delimitation of its frontiers or boundaries. This map has been provided by the authors.

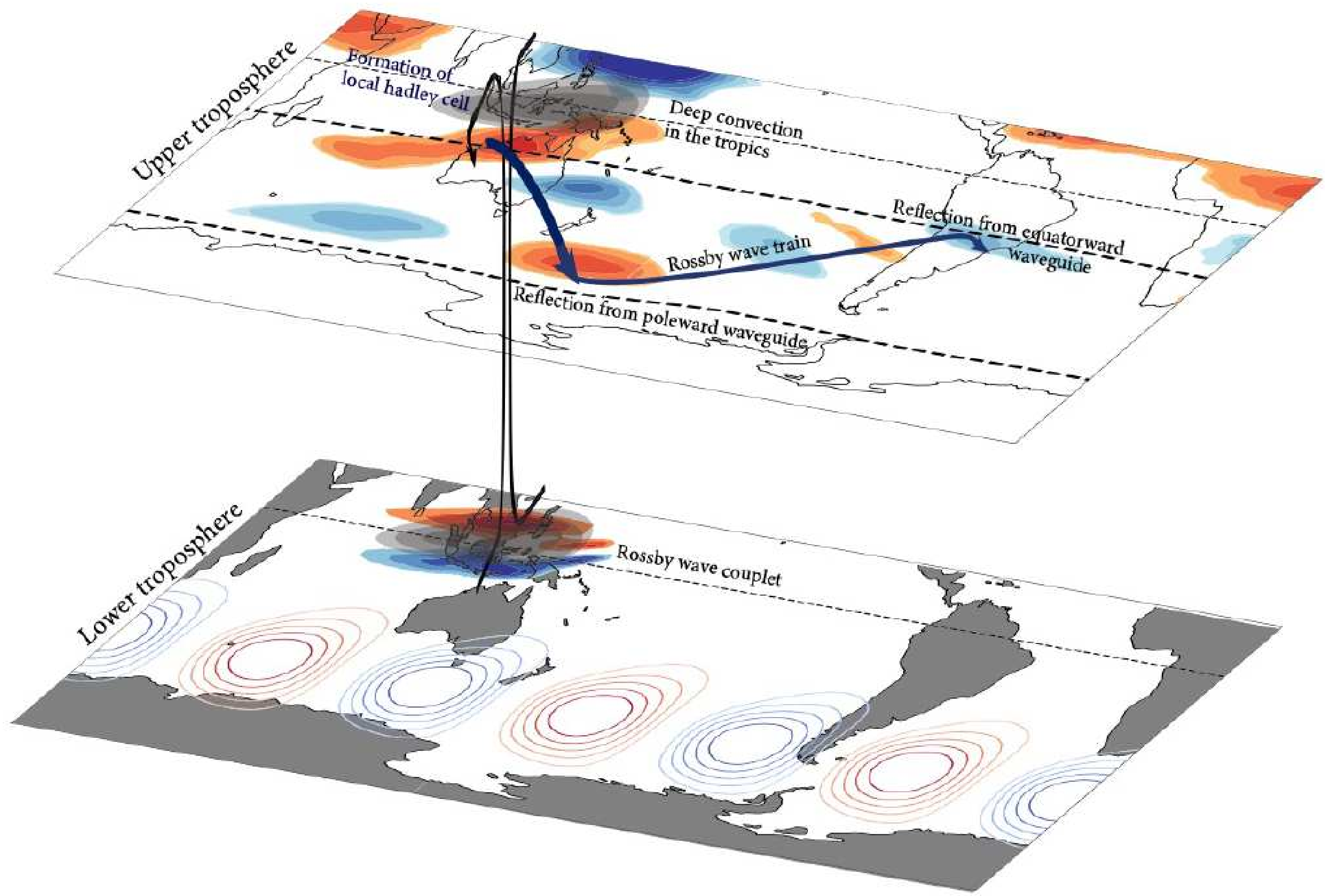

Figure 4

Schematic summarizing the role of tropical convection in generating Zonal Wave 3 in the Southern Hemisphere extratropics. Grey shading represents outgoing longwave radiation (OLR) and the vertical arrows represent deep convection in the tropics. Perturbation vorticity is shown by the coloured shading representing a Rossby wave train travelling poleward and eastward from the source region before

reflecting from the poleward and equatorward waveguides. The poleward and equatorward waveguides are represented by the thick dashed lines. Contours show the Fourier filtered zonal wave 3 from the 300hPa geopotential height field. Note: The designations employed and the presentation of the material on this map do not imply the expression of any opinion whatsoever on the part of Research Square concerning the legal status of any country, territory, city or area or of its authorities, or concerning the delimitation of its frontiers or boundaries. This map has been provided by the authors.

Supplementary Files

This is a list of supplementary files associated with this preprint. Click to download.

- GoyalSI.pdf